Hindawi
International Journal of Antennas and Propagation
Volume 2019, Article ID 1529656, 13 pages
https://doi.org/10.1155/2019/1529656

Research Article

Analysis of Performance Degradation Introduced by Radome for High-Precision GNSS Antenna

Jinyuan Liu, Lixun Li, Yong Zuo, Huaming Chen, and Shaojie Ni

College of Electronic Science and Technology, National University of Defense Technology, China

Correspondence should be addressed to Shaojie Ni; nishaojie123@126.com

Received 26 October 2018; Revised 18 January 2019; Accepted 6 February 2019; Published 2 June 2019

Academic Editor: Shiwen Yang

High-precision global navigation satellite system (GNSS) antennas employed on the fixed ground station are usually equipped with radomes, which are potential in yielding degradation of key parameters of antenna such as axial ratio and gain. This paper presents a study on the deterioration of high-precision GNSS antenna caused by the radome using electrically EM simulations including comparison of different geometries, materials, and heights of radome. Based on the study, an optimized radome model is proposed to minimize the axial ratio and gain degradation of antenna. Finally, a prototype of proposed radome is fabricated and measured. A good agreement between simulated and measured results evidently illustrates that the geometry, material, and height of radome are set appropriately.

1. Introduction

After decades of development, GNSS has been widely used as a powerful tool for many high-precision applications ranging from differential GPS to worldwide geodetic networks and aircraft control landing [1]. The GNSS antenna detects electromagnetic (EM) signals from multiple satellites, operating as a spatial and a frequency filter, and finally going through further processing by the receiver electronics [2], which is a crucial part to ensure the availability and accuracy of the system. GNSS signals near the surface of the earth are very weak (well below the receiver noise level), so it is significant that antennas provide sufficient gain over the entire upper hemisphere and must be right-hand circular polarization (RHCP) with good axial ratio [3]. To protect the enclosed antennas against adverse external environments (wind, rain, snow, and solar radiation) [4] and prevent long-term damage, GNSS antennas, particularly those employed on the fixed terrestrial applications, are usually equipped with dielectric radomes [5]. The effects of the radome on the enclosed antenna system are considerably complicated such as gain loss, boresight error, an increase in the sidelobe level, and distortion of the power pattern [6, 7], which are not negligible in many cases, in particular as far as high-precision applications are concerned including ground monitoring stations, geodetic mapping, seismic monitoring, and bridge deformation monitoring. Therefore, minimizing the EM performance degradation is the primary task in the design of a radome [8, 9].

The problem of predicting radome-induced degradations has been addressed recently by a number of researchers employing different approaches. Orta et al. [10] distinguish these approaches between direct and indirect methods. Among the former, the method based on the computation of the incident field on the inner radome surface followed by integration, on the outer surface, of the transmitted field is commonly known as ray-tracing method. This method assumes that the fields radiate from the antenna aperture like a bunch of rays and transmit through the radome as the wall is locally plane at each intercept point [11]. Moreover, ray techniques have been widely used for describing propagation through a radome wall both in their classical form and by employing the recently proposed evolutionary concept such as 2D or 3D ray-tracing and complex ray-tracing [12–15].

Sheret et al. [16] present a novel approach involving a two-dimensional ray-tracing method simulation and an electrically small unit cell simulation in high-frequency structure simulator to give an optimal thickness result which ensure minimum impact on the performance of the antenna. Xu et al. [17, 18] have used a 3-D ray-tracing method to evaluate the radome performance parameters and reveal that the EM characteristic of inhomogeneous radomes is potential in realizing high-performance airborne radomes superior to traditional variable thickness radomes (VTR).

However, these works mainly focused on the streamlined radomes for airborne applications; therefore, the concerned EM performance can mainly be the transmission loss (TL), bore sight error (BSE), and insert phase delay (IPD) [19–21]. It should be pointed out that results of these radome designs for dynamic vehicles do not naturally signify equally good EM performance in the case of fixed ground installations for high-precision GNSS applications, since the critical parameters that affects the accuracy of GNSS measurements may become rather distinctive.

Gain and axial ratio are well-known metrics with which the performance of antennas used in GNSS is evaluated [22]. On the one hand, the main beam antenna gain may be reduced due to the reflection from the air-dielectric interface, refraction effects, and dissipation within the dielectric layers. This denotes the ability of the antenna to efficiently receive the very weak satellite signals will be decreased. On the other hand, GNSS transmits circular polarization signal hoping that the axial ratio is as small as possible. Moreover, the frequency of GNSS now extends from 1.166 GHz to 2.502 GHz [23] which the corresponding wavelength is approximately 120-273 mm much larger than the thickness of the radome. Hence, the EM wave transmitting through the dielectric slab may be unsuitable to be decomposed into parallel and perpendicular components, and the ray-tracing method cannot produce reasonably good results. To improve the availability of the navigation system and to reduce the geometric dilution of precision, it is significant that antenna performance does not degrade considerably especially at low elevations. Therefore, it is essential to carefully investigate and mitigate various effects of radome on the antenna performance, including comparison with different materials and structures of radomes.

In this paper, we are trying to contribute to an assessment of the impact of radomes on antenna performance based on electrically EM simulations. We propose to optimize radome parameters for GNSS high-precision antennas including material properties, geometry, and height to minimize the axial ratio and gain degradation of antenna performance without going through exhaustive and expensive experiments and measurements which would provide theoretical guidance in the design process. The remainder of this paper is organized as follows. In Section 2, the effects of geometry, material, and height of radome on the axial ratio and gain of high-precision GNSS antennas are analyzed, respectively, using the same antenna model by CST Microwave Studio. In Section 3, in order to verify the accuracy and efficacy of the optimization radome model presented in Section 2, the real object of the antenna-radome system is manufactured and the comparisons with measured and simulated results are reported. Finally, some useful conclusions are derived in Section 4.

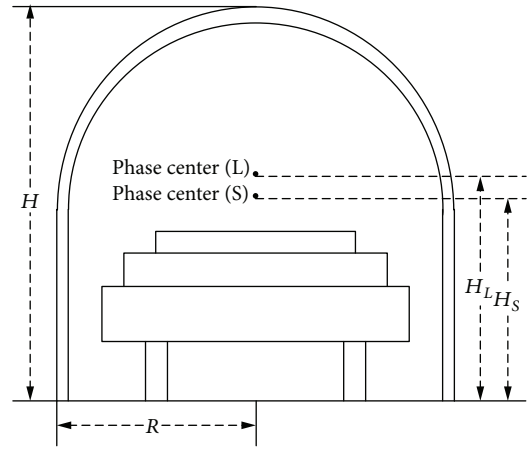

Figure 1: Antenna-radome system diagram.

2. Design for the L/S Radome

A high-precision GNSS antenna designed to place patch elements on the 3D choke ring is adopted as the simulation object. The antenna can provide superior performance extending from low L-band (1.166-1.289 GHz) and high L-band (1.554-1.612 GHz) to S-band (2.482-2.502 GHz), and the corresponding wavelength is approximately 120-273 mm. As shown in Figure 1, the base diameter and the height of the enclosed antenna are 360 mm and 180 mm, respectively. Moreover, the phase center of L-band (H_{L}) and S-band (H_{S}) are 192.9 mm and 182.7 mm, respectively. In this paper, the radome belongs to thin-wall monolithic structures with a wall thickness of 2 mm which is much less than wavelengths at operating frequency.

As earlier mentioned, the radome serves mainly as environmental protection of the antenna element. It must withstand harsh environment conditions such as wind, hail, extreme temperatures, and sun rays loading, which is often used for extended period of time (10-15 years for reference stations) [2]. Its geometry must prevent accumulation of precipitation and adherence of ice and water and prevent living creatures such as birds and small animals from sitting on or occupying it. Accordingly, it is important for radome to be hydrophobic and solid.

Moreover, when the phase center of the antenna is located at the center of the hemispherical radome, the radome has the least impact on the performance of the antenna, theoretically, since the electromagnetic wave entering the air-dielectric boundary can be considered as the normal incidence with every elevation angle which the angle of incidence is extremely small [24]. However, due to the phase centers of antennas at S-band and L-band differing by about 10 cm, the change in the height of the radome, that is, the relative position between the internal antenna and the radome wall, might also yield effects on the axial ratio and gain of the antenna in different frequency bands.

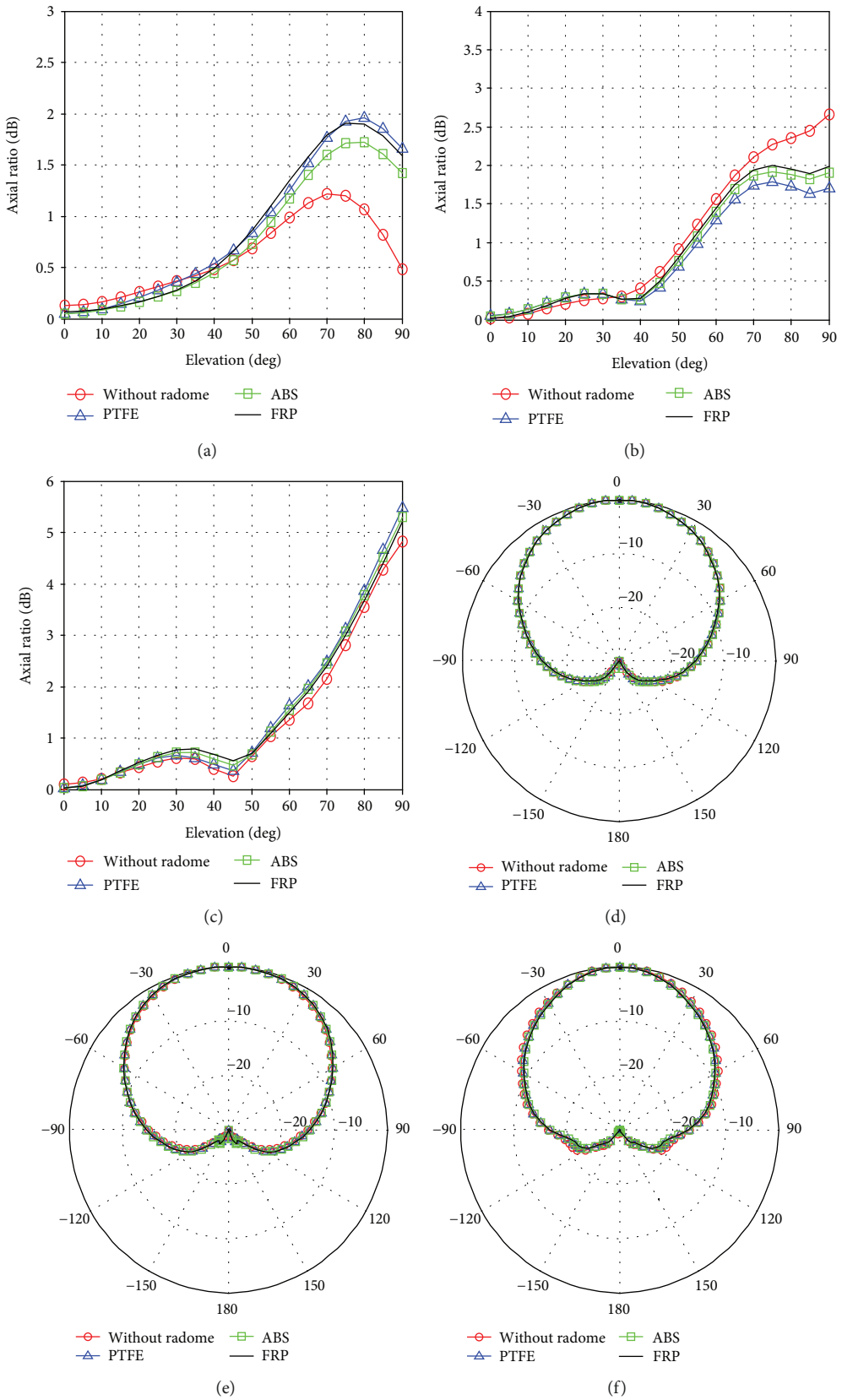

Figure 2: Simulated radiation characteristic comparison of antenna with different materials of radome: maximum axial ratio versus the elevation angle (a) at 1.22 GHz, (b) at 1.58 GHz, and (c) at 2.5 GHz; E-plane radiation pattern (co-pol) (d) at 1.22 GHz, (e) at 1.58 GHz, and (f) at 2.5 GHz.

Therefore, it is significant to choose the proper geometry, material, and height of radome for high-precision GNSS antenna. In order to provide a theoretical basis for the optimization radome model, the effects of geometry, material, and height of radome on the axial ratio and gain of antenna are demonstrated in this section.

2.1. Comparison of Different Materials. We select the hemisphere-cylinder radome with a height of 180 mm as the simulation object to have a further discussion in this section (see Figure 1). In analyzing radome electrical performance, it is important to evaluate the electrical properties of possible radome wall materials at various wavelengths. The primary electrical properties of candidate materials are the relative dielectric constant and the loss tangent of the candidate materials at the operational frequencies [25].

The axial ratio (AR) of a circularly polarized antenna at an elevation angle θ and azimuth angle φ is defined by

$$\mathrm{AR}(\theta, \phi) = \frac{|E_{\mathrm{R}}| + |E_{\mathrm{L}}|}{|E_{\mathrm{R}}| - |E_{\mathrm{L}}|}, \quad (1)$$

where E_{R} denotes RHCP components and E_{L} denotes LHCP components. As defined by (2), the axial ratio in the simulations denotes the maximum axial ratio of different azimuths ranging from 0° to 360° presented to be a metric of critical performance requirements expected from the antenna.

$$\mathrm{AR}(\theta) = \{\max(\mathrm{AR}(\theta, \phi)) | \phi \in (0, 2\pi)\}. \quad (2)$$

The axial ratio and gain characteristics of antennas under three frequency points selected from the specified frequency bands, that are, 1.22 GHz, 1.58 GHz, and 2.5 GHz, are used to analyze the effects of different materials on L-band and S-band, respectively, while antenna without radome is also introduced for comparison.

Figure 2 shows simulated radiation characteristic comparison of antenna with three different materials of radome including polytetrafluorethylene (PTFE), acrylonitrile-butadiene-styrene (ABS), and fiber-reinforced polymer (FRP). The relative permittivity and loss tangent of these materials are shown in Table 1.

Table 2 shows the peak gain (the elevation is 0 degree) of the antenna with three different materials of radome. As plotted in Figure 2 and Table 2, the gain characteristics of antenna with different materials of radome nearly stay the same under selected frequencies, whereas there are some slight differences on the axial ratio performances of antenna among different materials when frequency varies.

From Figure 2(a), it can be observed that the variation of radome materials have a little effect on the axial ratio of the antenna at 1.22 GHz when the elevation increases from 0° to 40° (the elevation on the horizontal plane is 90° in this paper), which the axial ratios are even less than 0.5 dB under all selected materials. Whereas with the elevation angle that varies from 40° to 90°, the axial ratios of antennas with radome obviously deteriorate compared with that of antenna without radome. Particularly, at the elevation angle of 75°, the axial ratio increases approximately 0.5 dB in the case of ABS material and 0.7 dB in the case of FRP material compared with that of antenna without radome, respectively.

Table 1: Characteristics of different materials.

Material	Relative dielectric constant	Loss tangent
PTFE	2.1	0.0002
ABS	3.1	0.003
FRP	3.7	0.005

Table 2: Peak gain of different materials of radomes at selected frequencies.

Material Peak gain Frequency	Without radome	PTFE	ABS	FRP
1.22 GHz	8.21 dBi	8.35 dBi	8.14 dBi	8.53 dBi
1.58 GHz	7.44 dBi	7.23 dBi	7.29 dBi	7.30 dBi
2.5 GHz	8.65 dBi	8.91 dBi	9.02 dBi	9.10 dBi

It can be seen from Figure 2(b), when the elevation angle is less than 40°, the axial ratios of antenna under different materials almost stay the same at 1.58 GHZ which are slightly larger than that without radome. However, when the elevation angle varies from 40° to 90°, the axial ratio of antenna without radome increases more rapidly, which improves approximately 0.5 dB compared to that in the case of PTFE material at the elevation angle of 75°.

As shown in Figure 2(c), the axial ratios of antennas under dielectric radome tend to degrade compared with that without radome. When the elevation angle is less than 50°, the axial ratios of antenna gradually deteriorate with the increase of the relative permittivity of radome materials at 2.5 GHz. However, on the contrary, the FRP and ABS materials are slightly better than PTFE when the elevation changes from 50° to 90°.

According to the results from Figure 2, there will be no distinctive differences on the axial ratio performance of antenna among three different materials, although PTFE and ABS materials have smaller relative permittivity than FRP. Nevertheless, it should be pointed out that the manufacturing difficulties and the cost of PTFE and ABS materials are much larger than FRP material which has more excellent mechanical properties, such as strength and hardness, and erosion resistance. Moreover, the deterioration of axial ratio of radome using FRP material do not exceed 3 dB for all operating frequencies when the elevation is less than 75°, which is within an acceptable range. Accordingly, FRP which is a light-weight, high-strength, and low-cost material would be a good choice as the material for radome of high-precision GNSS applications.

2.2. Comparison of Different Geometries. Several geometries of radomes are suited to high-precision GNSS applications

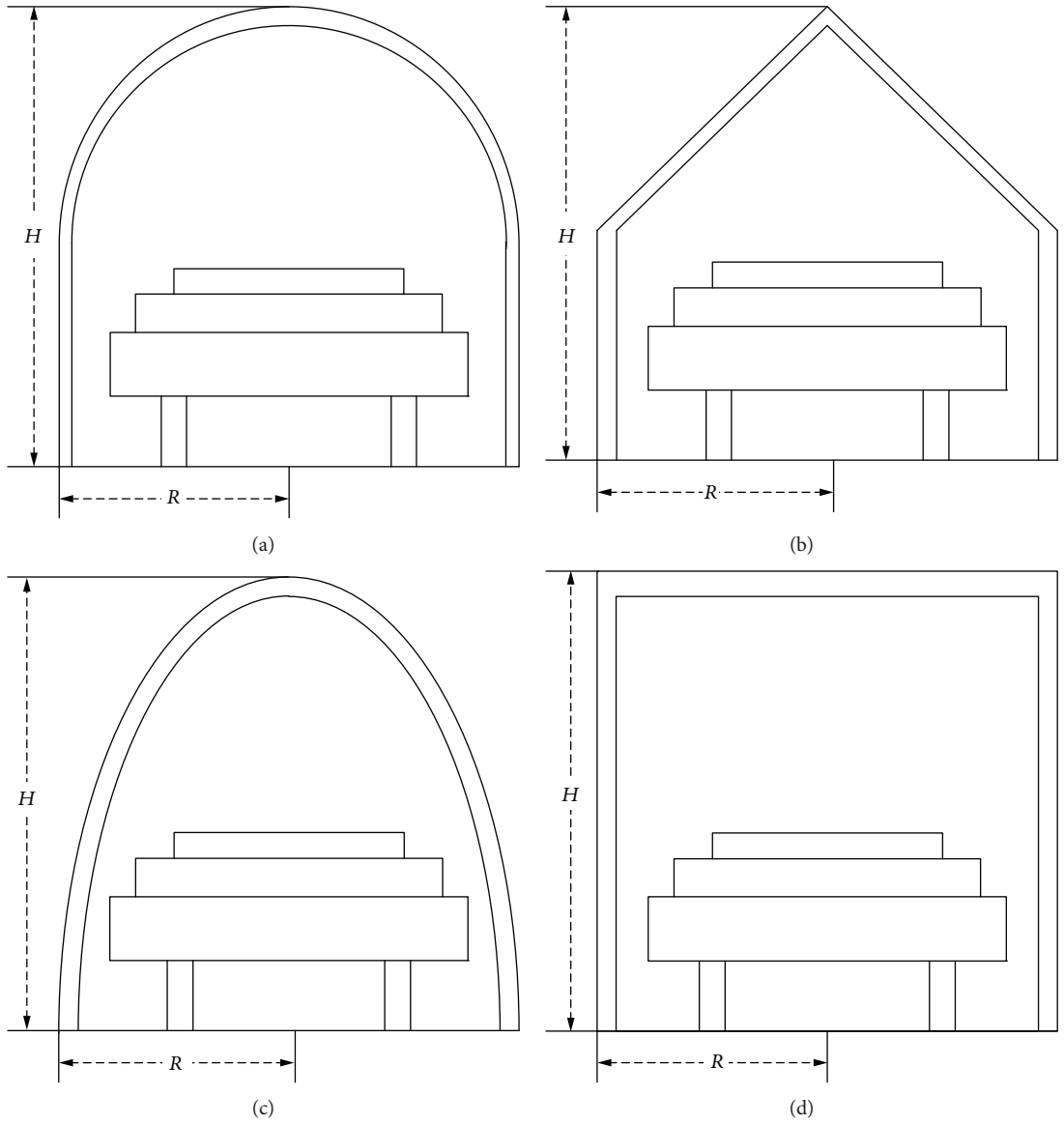

Figure 3: Different geometries of radomes: (a) hemisphere-cylinder radome, (b) cone-cylinder radome, (c) tangent-ogive radome, and (d) square radome.

depicted in Figure 3. As shown in Figures 3(a) and 3(b), the upper portions are hemisphere and cone, respectively, followed by a cylinder section with a height of H equal to 360 mm and a radius of R equal to 180 mm. The tangent-ogive radome which is also commonly used for airborne applications is shown in Figure 3(c), and the square radome is shown in Figure 3(d). The axial ratio and gain characteristics of antennas under three frequency points selected from the specified frequency bands, that are, 1.22 GHz, 1.58 GHz, and 2.5 GHz, are used to analyze the effects of different geometries on L-band and S-band, respectively. According to the analysis in Section 2.1, all the materials of radome are fiber-reinforced polymer (FRP) in this section.

The simulated radiation characteristic comparison of antenna with different geometries of radome is presented in Figure 4, while antenna without radome is also introduced for comparison.

Table 3 shows the peak gain of the antenna with different geometries of radome. From Figures 4(d)–4(f) and Table 3, it can be observed that there are slight differences on the gain of antenna among the different geometries of radome under all selected frequencies.

As shown in Figure 4(a), when the elevation angle is less than 60°, the axial ratios of antennas with these different geometries of radome are almost identical to that of antenna without radome at 1.22 GHz apart from the square radome. As the elevation increases from 60° to 90°, the axial ratio under square radome deteriorates much more than other cases, while the cone-cylinder radome is slightly better than other radomes.

It can be seen clearly from Figure 4(b) that the hemisphere-cylinder is better than other geometries of

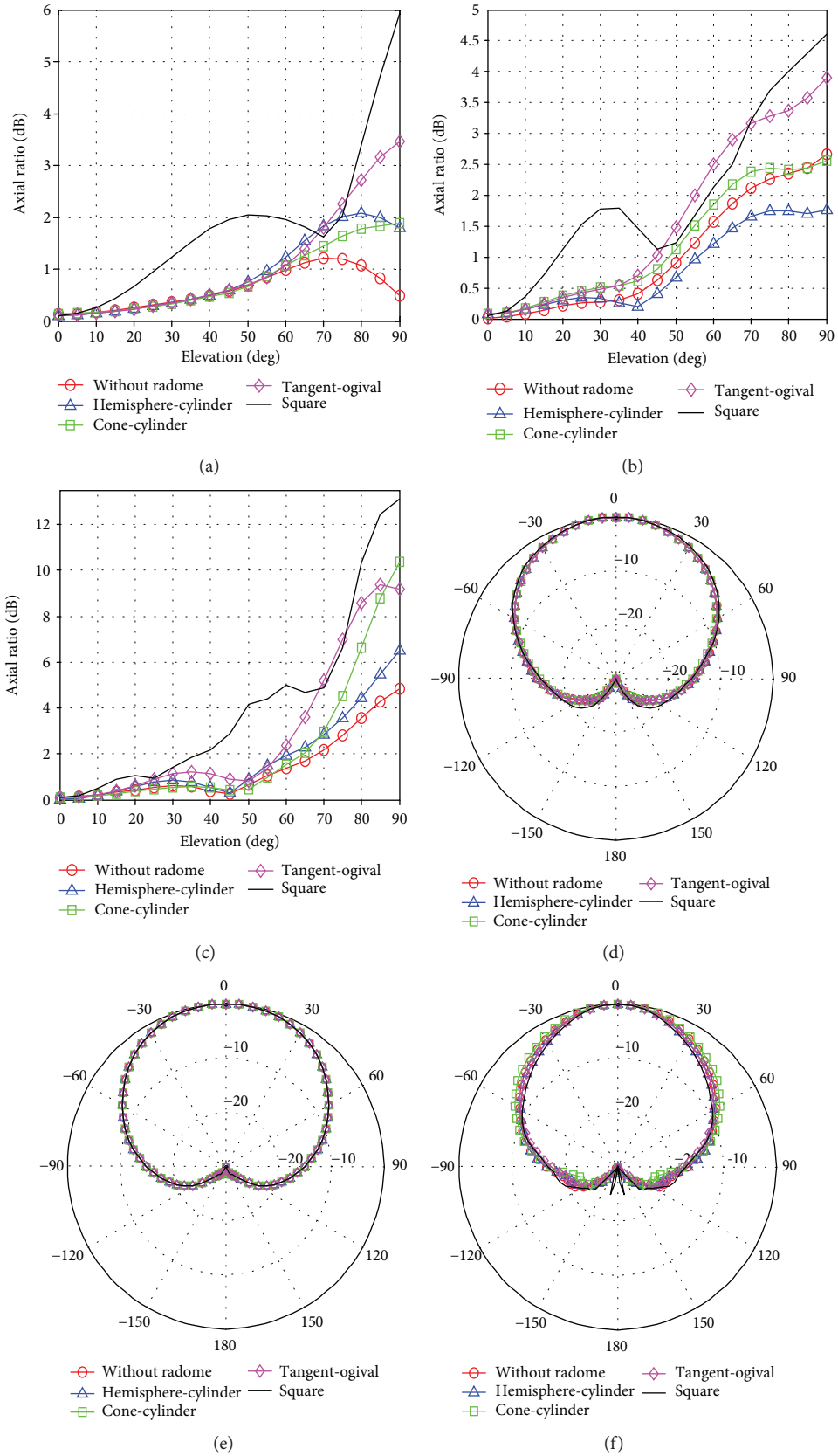

Figure 4: Simulated radiation characteristic comparison of antenna with different geometries of radomes: maximum axial ratio versus the elevation angle (a) at 1.22 GHz, (b) at 1.58 GHz, and (c) at 2.5 GHz; E-plane radiation pattern (co-pol) (d) at 1.22 GHz, (e) at 1.58 GHz, and (f) at 2.5 GHz.

Table 3: Peak gain of different geometries of radomes at selected frequencies.

Geometry Peak gain Frequency	Without radome	Hemisphere-cylinder	Cone-cylinder	Tanger-ogival	Square
1.22 GHz	8.21 dBi	8.09 dBi	8.323 dBi	8.06 dBi	7.68 dBi
1.58 GHz	7.44 dBi	7.25 dBi	7.30 dBi	7.36 dBi	6.44 dBi
2.5 GHz	8.65 dBi	8.83 dBi	8.09 dBi	8.99 dBi	9.22 dBi

radome at 1.58 GHz, especially when the elevation is larger than 40°, of which the axial ratio is even less than that without radome. This interesting phenomenon is notable that the dielectric wall may improve the axial ratio performance of antennas under some conditions which may still be a potential research area.

As plotted in Figure 4(c), the axial ratios improve rapidly with the increase of elevation angle under all selected geometries of radome, while the cone-cylinder, tangent-ogive, and square radomes deteriorate much more seriously as the elevation is larger than 70° which even exceed 6 dB. It should be noted that in high-precision GNSS applications, it is crucial for the axial ratio of antenna to be less than 6 dB to ensure good polarization performance of signal received by antenna.

According to the results from Figure 4, it can be concluded that the radiation characteristics of antenna with hemisphere-cylinder radome are better than that of antenna with cone-cylinder, tangent-ogive, or square radome. Therefore, the hemisphere geometry will be a better choice for high-precision GNSS antenna.

In theory, the hemispherical-shaped radome has more advanced properties for GNSS antenna in comparison of other common shapes such as tangent-ogive and cone: (1) the angle of incidence into the plane of radome is relatively small and generally less than 40° permitting low loss wall designs, (2) because of the symmetry, the angles of incidence only have very small changes with the azimuth angle of the antenna which is determined by the elevation angle combined with the normal line of radome, and (3) the hemispherical shape will ensure that signal distortion introduced by the radome is uniform for all angles and hence acts like a bias that is easily removed in the receive software.

2.3. Comparison of Different Heights. According to the results mentioned above, the hemisphere-cylinder radomes made of FRP material are adopted as the simulation objects to demonstrate the impact of height of radome on the radiation characteristic including the height of 250, 310, 345, and 360 mm, while antenna without radome is also introduced for comparison. It should be pointed that the radius of the upper hemisphere of the radome has not changed, that is, the height of the cylindrical part of radome is varied from 70, 130, and 165 to 180 mm. Figure 5 shows simulated radiation characteristic comparison of antennas with different heights of radome.

Table 4 shows the peak gain of the antenna with different heights of radome, which indicated this metric of antennas under different heights of radome has little variation. From Figures 5(d)–5(f), it can be observed that there are slight differences on the gain of antenna among the different heights of radome under all selected frequencies.

As shown in Figure 5(a), when the elevation angle changes from 0° to 50°, the variation of the height of the radome has little effect on the axial ratio performance of the antennas at 1.22 GHz, which the axial ratio is less than 1 dB under all selected height. Whereas, when the elevation angle is larger than 50°, 310 mm radome is better than other cases which have slight differences.

It can be seen from Figure 5(b) that, as the elevation angle increases, the axial ratio of the antenna gradually increases under the selected height of radome at 1.58 GHz. Especially, the axial ratio under 310 mm radome is significantly worse than that without the radome, and the axial ratio performance under 345 mm and 360 mm radome is much closer to that without the radome. By contrast, the axial ratio under the 250 mm radome is significantly smaller than that without radome even keeping below 1 dB under all elevation, which indicates that the antenna dielectric cover has an axial ratio improvement to the antenna at 1.58 GHz.

It can be observed from Figure 5(c) that, as the elevation angle increases, the axial ratio of the antenna under the of 250 mm and 310 mm radomes is more severely deteriorated at 2.5 GHz, especially when the elevation angle is larger than 40°, which even reach at 9 dB and 7 dB, respectively. As mentioned earlier, in high-precision GNSS applications, the axial ratio of antenna is required to be less than 6 dB to ensure good signal reception performance. By contrast, the axial ratio performance of antenna of 345 mm radome is much closer to that without the radome. Particularly, when the elevation angle is 75°, the axial ratio of the antenna is only about 3 dB.

Theoretically, as the height of the radome increases, the relative distance between the antenna phase center and the center of radome becomes smaller while the incident angle of the electromagnetic wave on the radome wall would be smaller and the deterioration of radome on the antenna performance will decrease at the same elevation angle. The axial ratio under 345 mm radome is better than that under 360 mm radome as shown in Figure 5(c), since the actual phase center of antenna in the simulation exists deviation which is not exactly located at 180 mm from the base of antenna. Because the phase centers of antennas in

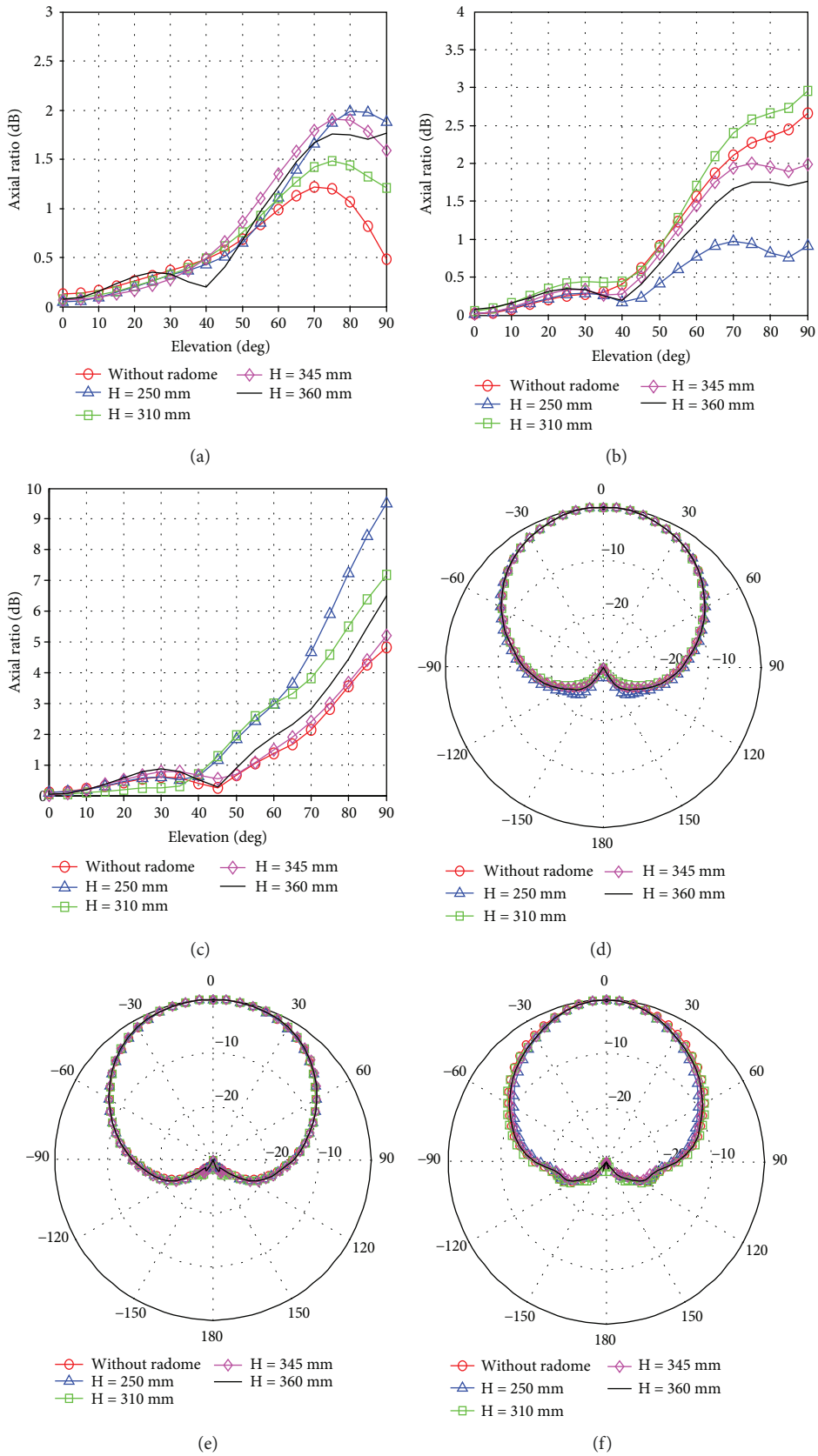

FIGURE 5: Simulated radiation characteristic comparison of antennas with different heights of radome: maximum axial ratio versus the elevation angle (a) at 1.22 GHz, (b) at 1.58 GHz, and (c) at 2.5 GHz; E-plane radiation pattern (co-pol) (d) at 1.22 GHz, (e) at 1.58 GHz, and (f) at 2.5 GHz.

Table 4: Peak gain of different heights of radomes at selected frequencies.

Height Peak gain Frequency	Without radome	250 mm	310 mm	345 mm	360 mm
1.22 GHz	8.21 dBi	7.69 dBi	8.37 dBi	8.53 dBi	8.09 dBi
1.58 GHz	7.44 dBi	7.52 dBi	7.25 dBi	7.30 dBi	7.25 dBi
2.5 GHz	8.65 dBi	9.24 dBi	8.64 dBi	9.10 dBi	8.83 dBi

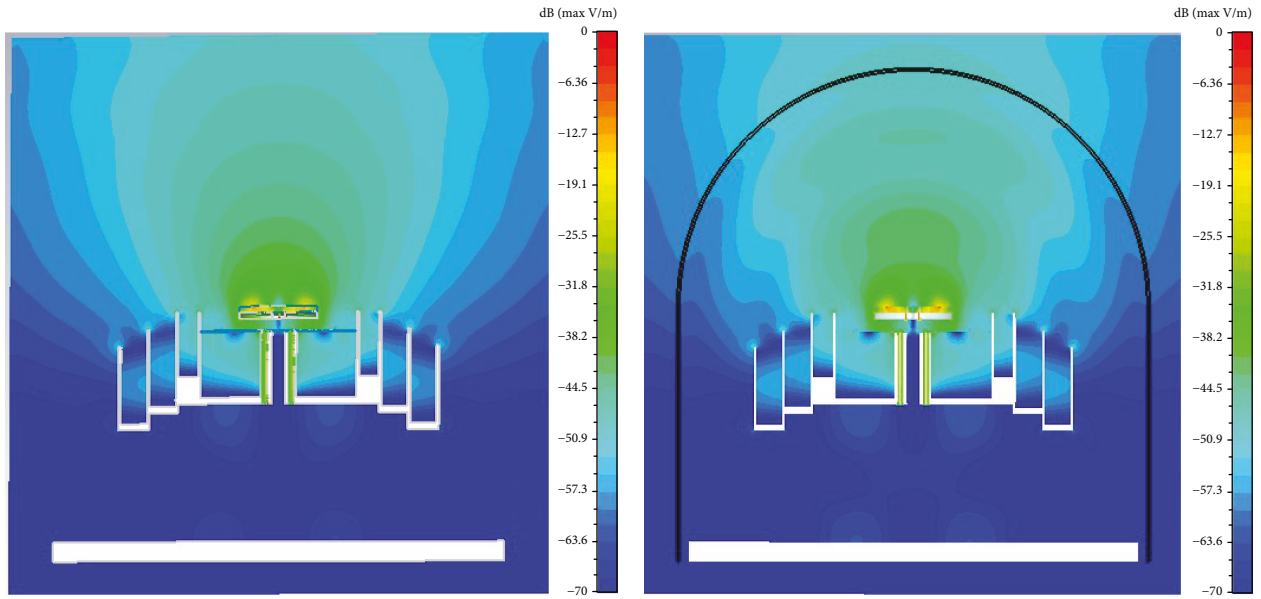

(a) (b)

Figure 6: Comparison of simulated electric filed distribution near the antenna at 2.5 GHz (a) without radome and (b) with radome.

(a) (b)

Figure 7: Photograph of fabricated proposed (a) radome and (b) antenna.

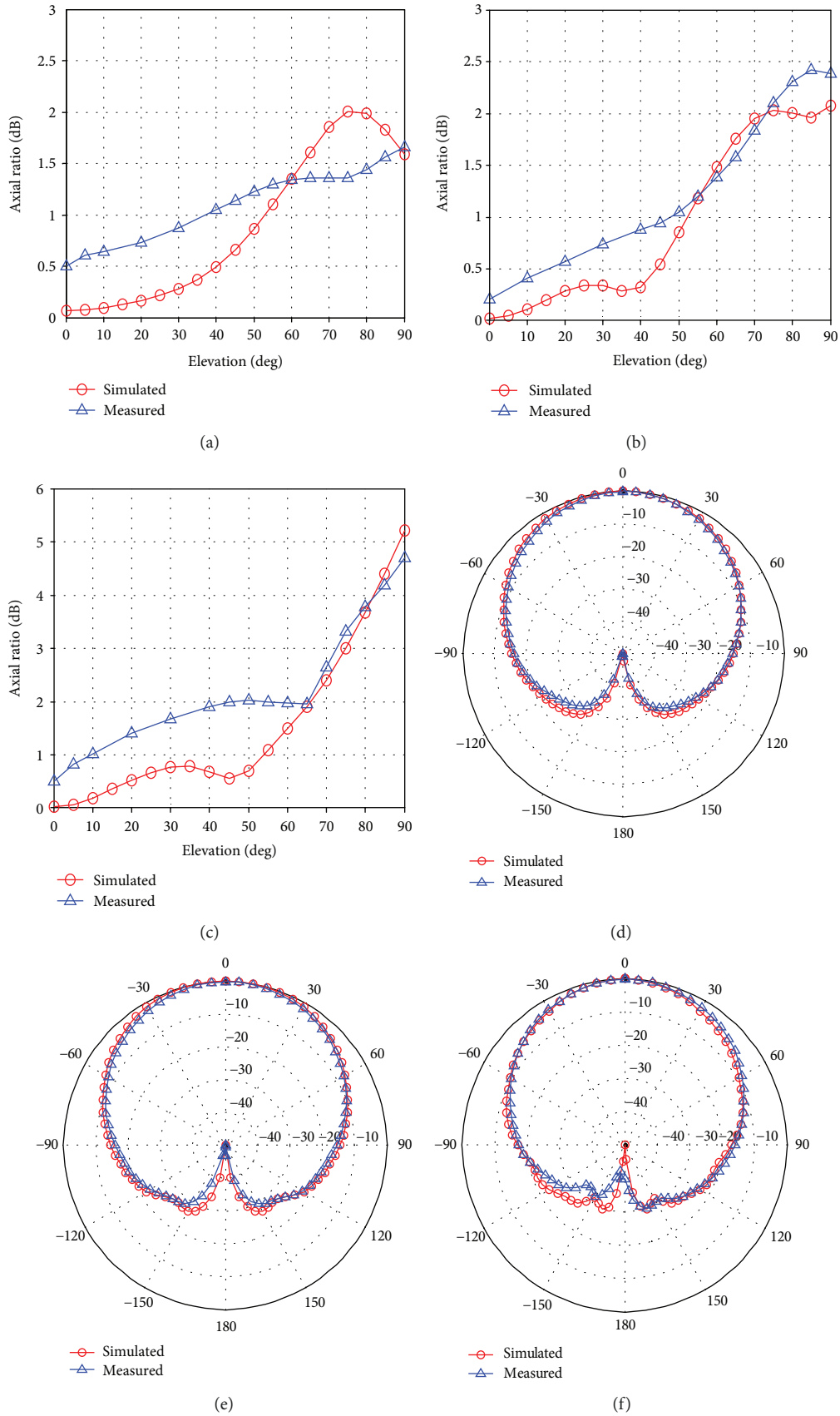

Figure 8: Comparison of simulated and measured radome: maximum axial ratio versus the elevation angle (a) at 1.22 GHz, (b) at 1.58 GHz, and (c) at 2.5 GHz; E-plane radiation pattern (co-pol) (d) at 1.22 GHz, (e) at 1.58 GHz, and (f) at 2.5 GHz.

the S-band and L-band and operational frequencies are different, the results from Figures 5(a) and 5(b) may not fully satisfy the tendency like Figure 5(c). However, we can observe that the axial ratios of antennas under all selected heights in the L-band (1.22 and 1.58 GHz) are below 3 dB within an acceptable range; hence, differences among the different heights at L-band could be relatively slight.

Several conclusions can be drawn from Figure 5 that the axial ratio performance of the antenna under 310 mm radome is relatively poor, while 250 mm radome can improve the axial ratio in the low-L frequency band, but the axial ratio in the S-band is out of the acceptable range for high-precision GNSS applications; 345 mm and 360 mm radomes both can cater to the requirements; however, excessive height of the radome may weaken radiation efficiency and improve the expense to fabricate. Therefore, 345 mm radome can provide more suitable performance in both L- and S-bands which the antenna axial ratio is less than 3 dB particularly when elevation angles vary from 0° to 75° which is the most concerned range in the GNSS applications. Therefore, for FRP material, a design with a height of slightly less than 360 mm locating the phase center of antenna close to the center of hemisphere can yield good performance which can probably be an acceptable optimization radome model.

3. Prototype and Measurement

Firstly, due to the radome located at the near field of antenna, to evaluate the effects of the proposed radome on the antenna in the near field, the electric field distributions near the antenna are simulated by CST Microwave Studio. The electric field distributions at 1.22, 1.58, and 2.5 GHz are similar, so only the electric field distributions near the antenna without and with radome at 2.5 GHz are shown in Figures 6(a) and 6(b) for brevity, respectively. Figure 6 demonstrates that, after adding the radome to the antenna, the radiation is deflected near the radome. The radiation is relatively weak, i.e., the radome can reduce the energy; however, the differences between the antenna with and without radome are slight. The results validate that the radome has little effect on the near-field characteristics of the antenna.

Furtherly, to check the validity of our analysis, according to the design parameters from Section 2, we fabricated a hemisphere-cylinder radome made of FRP material with the thickness of 2 mm, height of 345 mm, and width of 360 mm (see Figure 7(a)). We adopted color gel coat for the exterior of radome and alkali-free cloth and surface felt for fiber material. It can withstand common acid and alkali environment, ensure salt spray resistance on the surface, and can be resistant to marine atmospheric corrosion. Under strong ultraviolet radiation, it will not blister or crack for 5 years. And we measured the radiation of the L/S antenna (see Figure 7(b)) enclosed by the radome. The simulated and measured axial ratios and gains are shown in Figure 8 and Table 5.

As shown in Table 5, the measured peak gains are smaller than the corresponding simulated values due to the transmission loss such as reflection from the air-dielectric interface, refraction effects, and dissipation within the dielectric layers and the fabricated errors. Note that the differences between the measurement and simulation at 1.22 GHz and 1.58 GHz, respectively, are much larger because the manufacturing errors of the power divider and phase shifter working from 1.2 GHz to 1.6 GHz are considerable leading to the degradation of the fabricated antenna in the L-band is troublesome.

Table 5: Peak gain of measured and simulated radomes at selected frequencies.

Meas./simu. Peak gain Frequency	Measured	Simulated
1.22 GHz	8.53 dBi	11.16 dBi
1.58 GHz	7.30 dBi	9.13 dBi
2.5 GHz	9.10 dBi	9.63 dBi

Considering fabrication errors and uncertainties of radome such as changes in the dielectric constant, thickness of dielectric wall, and the surface roughness which are unavoidable in the fabrication process of the proposed radome, slight shift of axial ratio exists between the simulated and measured results as shown in Figure 8. It should be pointed that large variation of axial ratio between simulation and measurement results over the elevation ranging from 0° to 50° can be observed in all the three cases. To better illustrate this phenomenon, we remove the choke ring portion of the L/S antenna as shown in Figure 9(a). And the L/S antenna without the choke ring which is presented by Figure 9(b) is simulated under the same radome for comparison. And the axial ratio characteristic comparison of antenna with and without the choke ring at 2.5 GHz is presented in Figure 10. According to the results from Figure 10, the choke ring increases the axial ratio of antenna as the elevation ranging from 60 to 90 degrees. In theory, this is because the structure of choke ring increases the reflection of electromagnetic waves, especially in the case of high elevation angles. When the electromagnetic wave transmits into the radome, part of energy would reflect by the surface of the antenna including the choke ring and return to the inner wall of the radome then accepted by antenna leading to the enhancement of cross-polarization component which will deteriorate the axial ratio of the antenna.

4. Conclusion

This paper provides an optimized radome model for high-precision GNSS antenna avoiding degradation of the antenna performance as much as possible. To derive reasonable parameters of radome, the radiation characteristic comparison of antenna with different geometries, materials, and heights of radomes is presented by a series of numerical simulations. The simulation results proposed that the hemisphere-cylinder radome comprised FRP material with a height of 345 mm is a better choice

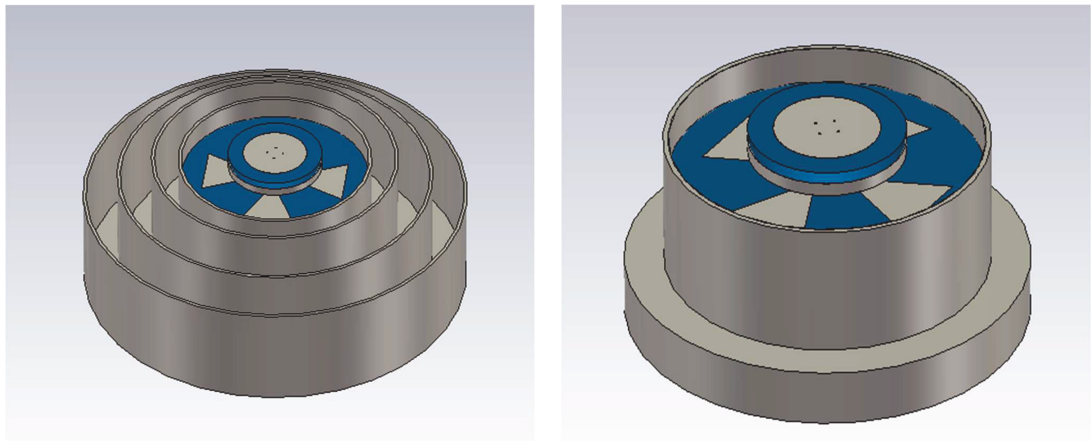

(a) (b)

Figure 9: (a) L/S antenna with the choke ring; (b) L/S antenna without the choke ring.

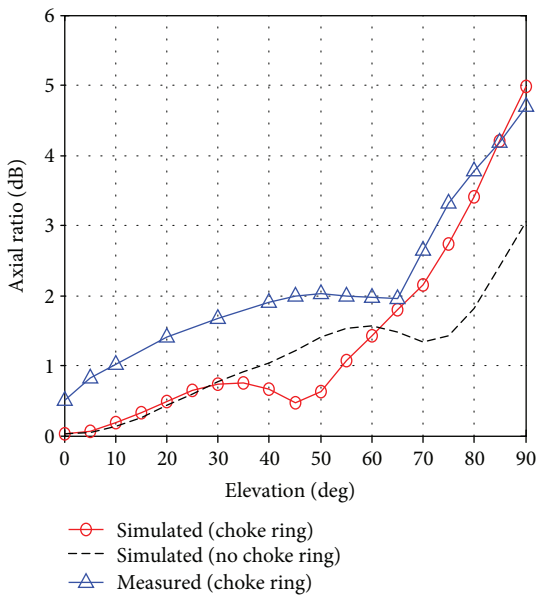

Figure 10: Comparison of simulated with/without choke ring and measured radome: maximum axial ratio versus the elevation angle at 2.5 GHz.

compared with other cases. Measured results of the fabricated radome prototype show that the axial ratio of enclosed antenna is less than 6 dB under all elevations, especially less than 2 dB when the elevation varies from 0° to 60° at all selected frequency bands. It proves the antenna-radome system possesses good circular polarization performance in both L-band and S-band.

Data Availability

No data were used to support this study.

Conflicts of Interest

The authors declare that there is no conflict of interests regarding the publication of this paper.

Acknowledgments

This work was supported by the National Natural Science Foundation of China (no. 41604016).

References

[1] L. Boccia, G. Amendola, and G. di Massa, "Performance evaluation of shorted annular patch antennas for high-precision GPS systems," *IET Microwaves Antennas & Propagation*, vol. 1, no. 2, pp. 465–471, 2007.

[2] B. Rama Rao, W. Kunysz, R. Fante, and K. McDonald, "*GPS/GNSS Antennas*," Artech House, Norwood, MA, USA, 2012.

[3] J. L. Volakis, A. J. O'Brien, and C. C. Chen, "Small and adaptive antennas and arrays for GNSS applications," *Proceedings of the IEEE*, vol. 104, no. 6, pp. 1221–1232, 2016.

[4] P. Li, W. Pedrycz, W. Xu, and L. Song, "Far-field pattern tolerance analysis of the antenna-radome system with the material thickness error: an interval arithmetic approach," *IEEE Transactions on Antennas and Propagation*, vol. 65, no. 4, pp. 1934–1946, 2017.

[5] T. Ning, G. Elgered, and J. M. Johansson, "The impact of microwave absorber and radome geometries on GNSS measurements of station coordinates and atmospheric water vapour," *Advances in Space Research*, vol. 47, no. 2, pp. 186–196, 2011.

[6] P. Li, W. Xu, and D. Yang, "An inversion design method for the radome thickness based on interval arithmetic," *IEEE Antennas and Wireless Propagation Letters*, vol. 17, no. 4, pp. 658–661, 2018.

[7] W. Xu, B. Y. Duan, P. Li, Y. Qiu, Z. Lin, and Y. Zong, "EM analysis of deformed metal space frame radome," *IEEE Antennas and Wireless Propagation Letters*, vol. 13, pp. 130–133, 2014.

[8] R. U. Nair and R. M. Jha, "Electromagnetic design and performance analysis of airborne radomes: trends and perspectives," *IEEE Antennas and Wireless Propagation Letters*, vol. 56, no. 4, pp. 276–298, 2014.

[9] W. Xu, B. Y. Duan, P. Li, Y. Zong, and Y. Qiu, "Novel compensation method for electromagnetic performance of dielectric radome based on reflector shaping," *IET Microwaves Antennas & Propagation*, vol. 9, no. 2, pp. 125–132, 2015.

[10] R. Orta, R. Tascone, and R. Zich, "Performance degradation of dielectric radome covered antennas," *IEEE Transactions on Antennas and Propagation*, vol. 36, no. 12, pp. 1707–1713, 1988.

[11] W. Xu, B. Y. Duan, P. Li, Y. Qiu, and Y. Zong, "EM performance analysis of radomes with material properties errors," *IEEE Antennas and Wireless Propagation Letters*, vol. 13, no. 1933, pp. 848–851, 2014.

[12] P. S. Mohammed Yazeen, C. V. Vinisha, S. Vandana, M. Suprava, and R. U. Nair, "Electromagnetic performance analysis of graded dielectric inhomogeneous streamlined airborne radome," *IEEE Transactions on Antennas and Propagation*, vol. 65, no. 5, pp. 2718–2723, 2017.

[13] R. U. Nair, M. Suprava, and R. M. Jha, "Graded dielectric inhomogeneous streamlined radome for airborne applications," *Electronics Letters*, vol. 51, no. 11, pp. 862-863, 2015.

[14] L. Zhou, Y. Pei, and D. Fang, "Dual-band A-sandwich radome design for airborne applications," *IEEE Antennas and Wireless Propagation Letters*, vol. 15, pp. 218–221, 2016.

[15] S. Narayan, G. Gulati, B. Sangeetha, and R. U. Nair, "Novel metamaterial-element based FSS for airborne radome applications," *IEEE Transactions on Antennas and Propagation*, vol. 66, no. 9, pp. 4695–4707, 2018.

[16] T. Sheret, C. Parini, and B. Allen, "Efficient design of a radome for minimised transmission loss," *IET Microwaves, Antennas & Propagation*, vol. 10, no. 15, pp. 1662–1666, 2016.

[17] W. Xu, B. Y. Duan, P. Li, and Y. Qiu, "Study on the electromagnetic performance of inhomogeneous radomes for airborne applications—part I: characteristics of phase distortion and boresight error," *IEEE Transactions on Antennas and Propagation*, vol. 65, no. 6, pp. 3162–3174, 2017.

[18] W. Xu, B. Y. Duan, P. Li, and Y. Qiu, "Study on the electromagnetic performance of inhomogeneous radomes for airborne applications—part II: the overall comparison with variable thickness radomes," *IEEE Transactions on Antennas and Propagation*, vol. 65, no. 6, pp. 3175–3183, 2017.

[19] R. U. Nair, S. Shashidhara, and R. M. Jha, "Novel inhomogeneous planar layer radome design for airborne applications," *IEEE Antennas and Wireless Propagation Letters*, vol. 11, pp. 854–856, 2012.

[20] W. Xu, P. Li, and Y. Qiu, "Electromagnetic performance analysis of inhomogeneous airborne radomes for circular polarization applications," *IEEE Antennas and Wireless Propagation Letters*, vol. 18, no. 1, pp. 74–78, 2019.

[21] W. Xu, B. Y. Duan, P. Li, and Y. Qiu, "A new efficient thickness profile design method for streamlined airborne radomes," *IEEE Transactions on Antennas and Propagation*, vol. 65, no. 11, pp. 6190–6195, 2017.

[22] K. A. Yinusa, "A dual-band conformal antenna for GNSS applications in small cylindrical structures," *IEEE Antennas and Wireless Propagation Letters*, vol. 17, no. 6, pp. 1056–1059, 2018.

[23] L. Li, Y. Huang, L. Zhou, and F. Wang, "Triple-band antenna with shorted annular ring for high-precision GNSS applications," *IEEE Antennas and Wireless Propagation Letters*, vol. 15, pp. 942–945, 2016.

[24] D. J. Kozakoff, *Analysis of Radome-Enclosed Antennas*, Artech House, 1997.

[25] P. Li, W. Xu, and S. Li-Wei, "Power pattern tolerance analysis of radome with the material property error based on interval arithmetic," *IEEE Antennas and Wireless Propagation Letters*, vol. 16, pp. 1321–1324, 2017.